coatings

MDPI

Article

Antireflection, Superhydrophilic Nano-Porous SiO_2 Coating based on Aerosol Impact Spray Deposition Technique for Solar PV Module

Kamran Alam [1,*], Saddam Ali [1], Abdul Saboor [1], Muhammad Salman [1], Maoz [1], Muhammad Humayun [2], Muhammad Sadiq [3] and Muhammad Arif [1,*]

1 US-Pakistan Center for Advanced studies in Energy, University of Engineering and technology Peshawar, Peshawar 25000, Pakistan
2 Department of Basic Science, University of Engineering and technology Peshawar, Peshawar 25000, Pakistan
3 Department of Mechanical Engineering, University of Engineering and technology Peshawar, Peshawar 25000, Pakistan
* Correspondence: Kalam3@asu.edu (K.A.); Muhammad.arif@uetpeshawar.edu.pk (M.A.)

Received: 4 July 2019; Accepted: 29 July 2019; Published: 6 August 2019

Abstract: In this research, silica nano-particles are deposited over the borosilicate glass and silicon wafer substrates by indigenously developed Aerosol impact deposition assembly using SiH_4, oxygen, and helium as precursors. The coating process involves deionization of gases leading towards nucleation sites for silica in the presence of plasma, while tuning the pressure difference between reaction and deposition chamber controls the coating thickness, porosity, and refractive index. The deposited coating layer on the substrate enhanced the transmittance to 99.6% at 600 nm wavelength. The induced porous nature and the graded index of the coated layer as observed from the AFM and SEM resulted in superhydrophilic behavior with a water contact angle of near to 0°. The super-hydrophilicity of the coating contains self-cleaning properties, suggesting an improvement of the performance of solar PV modules as well.

Keywords: antireflection coating; porosity; aerosol spray; silica nanoparticles

1. Introduction

A significant uptick has been noticed in the research on self-cleaning and antireflective coatings in recent decades. Their application is widespread, including photovoltaic solar panels, lasers, automobiles, optical instruments, and solar collectors [1–5], among others. Additionally, self-cleaning coatings play a major role in the design of photodetectors, sensors, and membrane technology [6–8]. The primary design concern in these instruments is high transparency; however, the performance of these instruments is inevitably degraded by incessant outdoor exposure and deposition of dust, wet snow, and bird droppings, leading to loss of transparency. Consequently, self-cleaning properties of coatings are gaining more importance in conjunction with improved antireflective properties [5,9]. For instance, a single dust storm can decrease the efficiency of a solar panel by up to 22% [10]. It has been noted that for a crystalline silicon solar photovoltaic module, a decrease in efficiency corresponding to each micrometer thickness of soiling is about 25%/μm for naturally deposited dust particles [11]. Self-cleaning antireflective coatings are, thus, deemed more advantageous in a diverse spectrum of applications owing to their resistance to dust accumulation, alleviating optical losses [12]. In solar PV modules, for instance, they could lead to a significant improvement in both the optical and electrical efficiency [10–12].

The antireflective behavior of antireflective (AR) coatings originates from the satisfaction of the destructive interference conditions for light waves reflected from the glass/coating and coating/air

surfaces, resulting in improved transmission [8,9]. This process, however, requires fine-tuning of the coating thickness to one-fourth of the incident light's wavelength ($\lambda/4 \times n_c$). At the same time, the refractive index (RI) of the antireflective coating (n_c) should meet the condition that n_c should be equal to $(n_s \times n_a)^{1/2}$, where n_s and n_a are the refractive indices of the substrate and air, respectively [10]. This means that for a glass substrate with RI of 1.5, the refractive index and thickness of the coating should be around 1.225 and 120 nm, respectively. However, materials with such a low refractive index do not exist in nature [13]. The materials that come closest to this value of refractive index are magnesium fluoride at 1.39 and silica at 1.46 [14]. A popular way around this problem is to introduce porosity in the material leading to a reduction in the refractive index of the material. For this reason, silica-based coatings have achieved significant focus in the development of antireflective coatings, owing to their abundant availability, higher accessible surface area, low cost, and low dielectric constant [14–16]. Current trends in AR coatings invariably involve one or more of the deposition techniques, such as etching, chemical vapor deposition (CVD), spray coatings, sol-gel method (spin or dip coating), layer-by-layer electrostatic self-assembly, and soft lithography. The key requirement of these coatings is the introduction of the porosity inside the coating to achieve a low refractive index value [17–20]. Some of these coatings have already been commercialized, prominent among which is the multilayer silica nanoparticle coating on glass using spin, dip, and roller coating techniques for PV applications [19]. Recent research has proposed numerous multifunctional coating mechanisms and diverse applications for such coatings [21–25]. Layer-by-layer coating deposition assisted by electrostatics is one such approach for deposition of nanoparticle and polyelectrolyte coatings on a multitude of substrates [17,18]. Aytug et al. [26] have developed three dimensionally crossed nanoporous coating, capable of Fresnel light reflection control, and improved transmission. They used the vapor deposition process on metastable spinodal phase-separated low-alkali borosilicate glass, and then performed differential etching of the surface to make the surface superhydrophobic. A water contact angle (WCA) greater than 160° was achieved, but transmittance was just over 95%. The process is complex, has many steps, and compromises the cost of the coatings [26]. Zhang et al. [27], on the other hand, were able to achieve 96.86%–97.34% transmission through a novel nano-composite of a silica–silica nanoparticle coating using sol-gel technique. The nanoparticles were deposited by dip coating. They achieved a suitable refractive index of 1.21 through fine-tuned deposition. The coating was superhydrophilic, with a water contact angle of less than 5, and showed excellent antifogging results. Wang et al. gauged the impact of surface roughness on the transmittance and wettability by comparing two coatings with varying surface roughness. They concluded that micro and nano hierarchical roughness coatings exhibited higher wetness stability, contrary to the low roughness surface. It was also found that with nanoscale roughness, the transparency of the coating is much better than at microscale. Therefore, there is a tradeoff between the transparency and wettability of the surface. Similarly, he showed that these super wetting surfaces help in corrosion control of different surfaces [28,29]. Similarly, Xu et al. achieved transmittance and water contact angle of 95% and 162°, respectively, by employing a lotus-leaf-like hierarchical structure [30]. The chemical composition of the coatings plays a significant role in the topography and mean roughness of the surface, as demonstrated by Carla et al. suggesting a 125–150 nm roughness value is prerequisite for attainment of super-hydrophobic properties [31]. Different chemical composition of the coating material leads to varying properties, for instance organo-silane compounds have been utilized to achieve super-hydrophobic silica coatings combined with Tetraethyl orthosilicate (TEOS) [32]. Cai et al. [33] employed methyl tri-ethoxysilane (MTES) and tri-methylethoxysilane (TMES), respectively, as precursors for hydrophobic antireflective and dip coating methods for fabrication. The water contact angle of the surface was increased from 22° to 108°. Michael et al. [34] used a chemical vapor deposition system to fabricate tri-layer $VO_2/SiO_2/TiO_2$ multifunctional antireflective coatings for energy saving window glass. The coatings showed very high transparency and high strength, but the use of Titania nanoparticles increased the refractive index above the optimum value. The coating was photocatalytic in nature but the water contact angle observed was near to 90°, which is not in the range of superhydrophobicity. These conventional

deposition techniques, however, suffer from the disadvantage of high material and equipment cost, limited material combinations, mass manufacturing, and stability, and low throughput. Sol-gel applied coatings, in particular, lack in durability once the solvent has evaporated in high temperature calcinations in many cases. These factors severely limit the application avenues of these coatings in areas where cost and durability is a major concern, such as solar PV [35].

In the context of the recent research on antireflective, self-cleaning coatings, this research presents a novel approach to nano-particulate porous silica coatings on glass and silicon substrates through aerosol impact spray deposition. The major advantage of this method is the added control offered for fine-tuning the porosity and the thickness of the thin film along with surface roughness. Unlike other synthesis methods, such as sol-gel, spin, and dip coatings, there is no issue of coating cracking in this process, as there is no solvent involved in the synthesis process. Along with the ease of fine-tuning parameters and high quality coatings, aids can be used to coat different materials other than silicon dioxide and its substrates, irrespective of shape and thickness. Thickness and porosity of the thin film coating can be tuned from 60 nm to several micrometers and from 50% to 90%, respectively [36]. A silica multilayer coating with a refractive index of as low as 1.05 can be made for different applications using aids. In addition, nanoparticle size can be tuned by increasing or decreasing the residence time of the precursors in the reaction chamber of the system. Therefore, this system has the capability to synthesize various sizes of different particle coatings for a whole range of wide applications. Due to the high impact speed (up to 1000 m/s) of the particle inside the deposition chamber, the particles adhere well to the substrate due to either chemical bonding or van der Waals interaction. This shows the scalability of this technique and its advantages in other synthesizing processes mentioned above. The enhancement of the optical and cleaning parameters of glass substrates shows the viability of these coatings. The morphology and surface analysis was also investigated using SEM, AFM, and FTIR. Due to the high porosity and controlled roughness of the film, the coated film was antireflective and super-hydrophilic in nature. The porosity and the surface roughness of the nanocomposite coatings gave rise to a decrease of the refractive index from 1.48 to 1.23 that ultimately helps in the antireflection and self-cleaning properties of the coated substrates.

In the following section, the materials and experimental procedures used in this research will be discussed briefly. Additionally, all of the characterization tools that are used in this research work will be discussed. Section 3 will discuss the results obtained from this research.

2. Materials and Methods

2.1. Materials

Borosilicate Glass slides and Silicon polished wafers (Sail Brand, Shanghai, China) with dimensions of 75 mm × 25 mm × 1 mm were used as the substrates. Sulfuric acid (H_2SO_4, 98 wt.%, AR), acetone (C_3H_6O, AR), and ethanol (C_2H_5OH, AR) were purchased from Sigma Aldrich (Karachi, Pakistan). Deionized water (>18 MΩ cm) was used in all cleaning and rinsing procedures. All reagents mentioned above were used without further purification.

2.2. Experimental Procedure

In this research work, borosilicate glass and silicon wafer substrates were used as substrates to deposit silica nanoparticle coatings. The deposition process commenced with cleaning of exposed surfaces of both of the substrates. At first the substrates were sonicated for 10 min in the presence of acetone followed by rinsing with deionized water. The cleaned substrates were dried by blowing nitrogen gas over all of the exposed surfaces at moderate pressure. Afterwards, the individual substrates were placed inside the indigenously developed aerosol spray assembly for the deposition of coating. The assembly comprises synthesis and deposition chambers separated by a variable nozzle aimed at expanding the precursor gases supersonically over the substrate, as demonstrated in Figure 1. The reaction chamber encompasses two rectangular electrodes of 15 cm height and 7 cm width, placed

parallel to each other at 1.5 cm apart, supplied with 0.98 W cm^{-2} RF power at a frequency of 13.56 MHz to generate plasma. The basic design of the reaction chamber is described elsewhere [37]. The 5% SiH_4 precursor was mixed with oxygen and helium at control flow rates of 160, 500, and 400 sccm, respectively, in the reaction chamber, where they were turned to silica nano-particles by the plasma. The reaction chamber pressure was maintained at 2–2.5 Torr. The newly formed nanoparticles were plunged through the 0.5-mm slit nozzle towards the substrate in the deposition chamber, which was maintained at a pressure of 0.2 Torr. The pressure ratio between the two chambers aids in controlling the density and porosity of the thin film on the substrate. Depending on the desired film thickness and refractive index, the substrate holder is moved back and forth several times at 10 cm s^{-1}. In this research work, the target was single layer coating of silicon dioxide nanoparticles with a refractive index, porosity, and thickness of 1.23, 50%, and 120 nm, respectively. Two sets of thin films were deposited on glass and silicon wafer substrates in the same condition for ease of characterization. The glass substrate film was subjected to UV-Vis-NIR transmission spectroscopy along with electrical performance assessment, whereas ellipsometry, electron microscopy, and FTIR analysis were performed on the silicon wafer. All the experimental steps are shown in Figure 2.

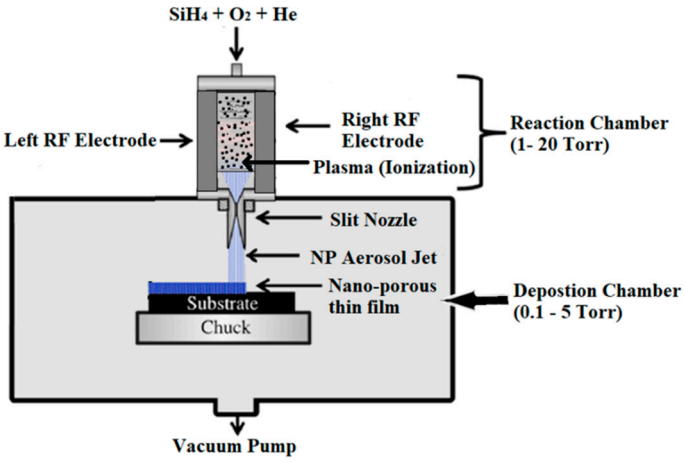

Figure 1. Aerosol spray deposition assembly.

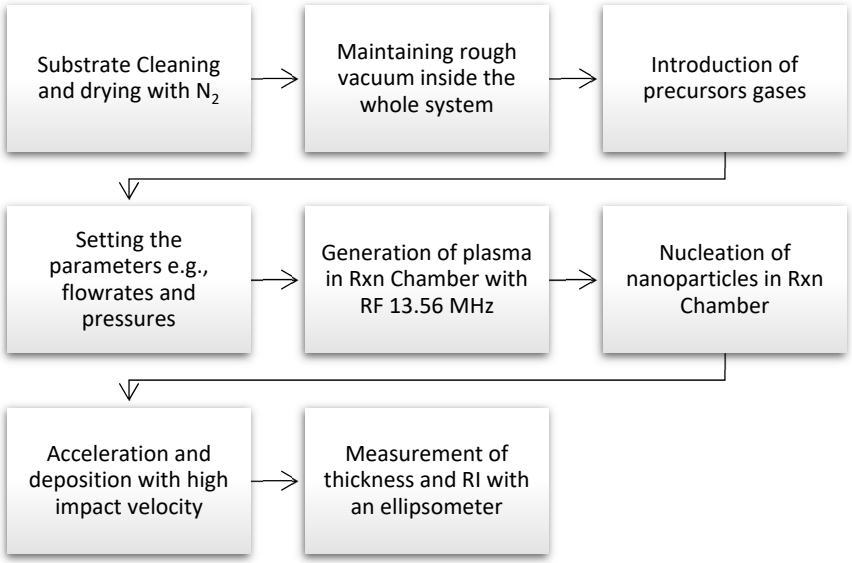

Figure 2. Experimental steps.

2.3. Characterization Techniques

Prior to experimental characterization, the theoretical transmission spectrum for the borosilicate glass was simulated using Sunsolve ray tracer software (v3.9.7) developed by PV Lighthouse for coated and uncoated substrates. The optimum film thickness and refractive index were estimated using Cauchy model [38], whereas Bruggeman effective-medium approximation [39] was adopted for optimum porosity determination. The broad range (300–1200 nm) transmission spectrum was recorded with a UV-NIR spectrophotometer (Lambda 950, Perkin-Elmer, Tempe, AZ, USA). Atomic force microscopy (scanning probe microscope (SPM), Bruker, Tempe, AZ, USA) was carried out in tapping mode with a nominal probe tip radius of 10 nm, scanning probe frequency of 512 Hz, and scan area size of 4 μm^2 to examine surface topography. The surface morphology and composition identification were observed by field emission scanning electron microscope (FEI Quanta FEG 450, Tempe, AZ, USA) coupled with energy dispersive X-ray spectroscopy (EDS). Surface bonding was identified using FTIR (IR tracer 100, Tempe, AZ, USA) analysis. To gauge the anti-soiling capabilities of coatings, the water contact angle measurements were conducted at ambient temperature using a KRUSS drop shape analyzer (DSA30, Tempe, AZ, USA) with a contact angle measuring precision of ±0.5°. The water contact angle estimation was done by dropping 4 µL of water over the substrate surface. The process was repeated at six different spots on the substrate for greater accuracy. Subsequently, the antifogging assessment of the coatings was carried out by lowering the temperature of the coated substrate to 18 °C for 3–6 h followed by exposure to ambient temperature at 30 °C, with 40% relative humidity.

3. Results and Discussion

3.1. Optical Modeling of the Coating

In principle, two mechanisms are used to achieve an AR effect in thin films. The first is by relying on a continuous graded refractive index material between the air and substrate material. The second is by using sufficiently thin films that can lead to destructive interference between the surfaces [5–7]. Reflection R for a glass plate with normal incident light intensity I_0 and transmitted light intensity I_T, while assuming no optical dispersion, is given in Fresnel's Law as Equation (1):

$$R = \frac{(n_1 - n_0)^2 + k^2}{(n_1 + n_0)^2 + k^2} \tag{1}$$

here, n_1 and n_0 are the real refractive indices of the substrate and air in the case of uncoated glass or the air and coating for coated glass, respectively. K represents the imaginary part of the refractive index, usually negligible in visible and near infrared ranges of the spectrum for borosilicate and the prevalent coating materials. This equation gives reflection losses of 4.5% for each side of the glass–air interface, amounting to a total loss of 8%–9%. However, the introduction of the antireflective coating leads to interference of the light reflected by the air-coating surface (R_2) and the coating–substrate interface (R_1). Also introduced is a phase shift (δ) of the wave, given by Equation (2):

$$\Delta = 4\pi n_c \, d/\lambda \tag{2}$$

where n_c and d are the coating refractive index and thickness, respectively, while λ represents the wavelength of the incident light. The resultant total reflectivity thus achieved by the combination of R_1 and R_2 and the incorporation of the entailed phase shift are given by Equation (3):

$$R_T = \frac{R_1^2 + 2R_1R_2\cos\delta + R_2^2}{1 + 2R_1R_2\cos\delta + R_1^2R_2^2} \tag{3}$$

when assessing the performance of the intended coating materials, the increase in the transmission estimated from the equations above is a good measure. The percent increase in the transmittance of

the substrate with the application of antireflection coating is obtained by subtracting Equations (1) and (3). It is also helpful to notice that destructive interference occurs when the condition $\delta = (2k - 1)\,\pi$ is met, with w being the order of destructive interference. Alternatively, the condition is also defined by Equation (4):

$$\frac{2(w-1)\lambda}{4} = n_c d \tag{4}$$

In cases where the condition in Equation (4) is true, the combination of Equations (2) and (4) gives a further simplified representation of phase angle; that is, $\cos\delta = -1$. The optimal antireflection condition is achieved when Equation (4) is fulfilled and R_1 becomes equal to R_2. Accordingly, we arrive at 2 conditions for optimal coating: $d = \lambda/4n$ and $n_c = (n_s)^{1/2}$.

3.2. *Antireflection Results*

The antireflection performance of the coating was assessed by estimating three quantities: transmittance spectrum, maximum transmittance, and the weighted average transmittance (Ts) at 300–1200 nm spectrum. Weighted average transmittance was calculated using Equation (5):

$$T_s = \frac{\sum_{\lambda\min}^{\lambda\max} T(\lambda) E_\lambda \Delta\lambda}{\sum_{\lambda\min}^{\lambda\max} E_\lambda \Delta\lambda} \tag{5}$$

where λ_{max}, λ_{min}, $T(\lambda)$, E_λ, and $\Delta\lambda$ represents the longest wavelength, the shortest wavelength, the wavelength-dependent transmittance, the solar irradiance intensity, and the wavelength increment, respectively.

Figure 3 presents the simulation and experimental transmittance results of the uncoated and coated glass slides (black for uncoated sample, green and red for coated sample) in the wide range of 300–1200 nm. An average transmittance of 90.1% was observed for the bare glass. The average transmittance after silica coating deposition was more than 97% for normal incidental light. The average increase in the transmittance in the 300–1200 nm range of the spectrum was found to be 6.3% when measured in the laboratory, while an increase of 6.9% was found in simulation. A peak transmittance of 99.8% was recorded at 550 nm for a simulated refractive index of 1.23 and thickness of 120 nm, although the peak is lower at higher wavelengths. On the other hand, in experimental results, a peak value of 99.6% was achieved at 600 nm. As can be witnessed from the curves, the experimentally measured transmittance in some areas is lower than the simulated curve. This may be due to the slightly higher refractive index and thickness of the developed coatings in the laboratory than the design values. In addition, a slight increase of absorption edge in the blue band in the coated curve may be due to the very small size of silica nanoparticles, as mentioned by Rahman et al. in their work [40].

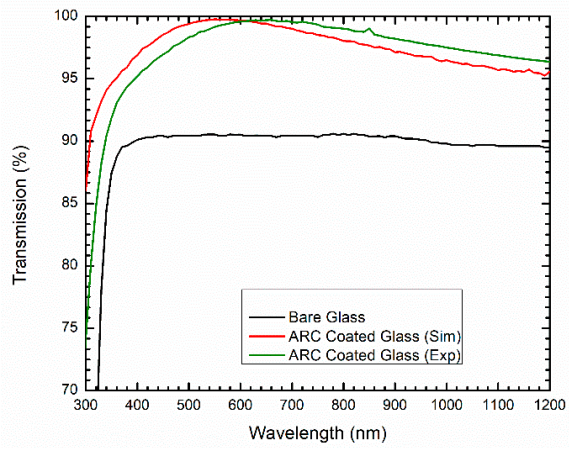

Figure 3. Transmission spectra of Coating.

3.3. FTIR Spectra Analysis

For assessment of the absorption in the IR region, and to find out which functional groups are attached on the surface of the coatings, FTIR was performed as shown in Figure 4. Results of FTIR curve show an appreciable absorption band at 1080 cm^{-1} owing to the stretching modes of the Si–O–Si group. Another strong band at 790 cm^{-1} corresponds with the bending vibration of Si–$(CH_3)_3$. The broad band at 3700–3200 cm^{-1} and the small peak at 1650 cm^{-1} points to the stretched band of hydroxyl group Si–OH on the surfaces of silica nanoparticles. It has already been established that the wettability of the surface depends upon the chemistry of the surface [21]. The presence of the OH group at the surface quickly attracts and spreads the water droplets due to hydrogen bonding, and thus becomes a thin film. Due to the spreading of the water droplet, the dirt or contamination on the surface is also removed with the water, thus removing the dust from the surface. The strong OH group also indicates that the majority of Si atoms are present at the surface. During the deposition process, these surface groups react with each other to produce Si–O–Si bonds via condensation [35]. Thus, FTIR confirms the presence and stretching of the hydroxyl group and the concomitant of hydrogen bonding, ultimately creating superhydrophilic behavior.

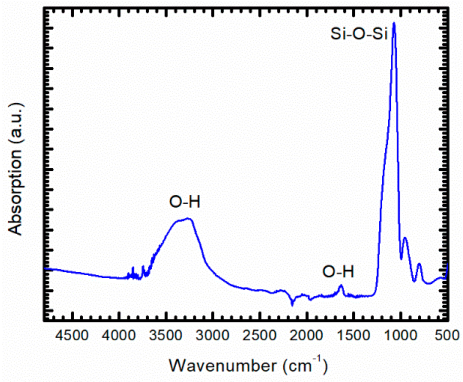

Figure 4. FTIR spectra of the coating.

3.4. Antifogging Results

Superhydrophilic nanoporous coatings have the ability to effectively eliminate water condensation into droplets on substrates. Formidable superhydrophilic properties leading to antifogging behavior were noted in the developed silica nanoparticles. As evident in the Figure 5 below, the silica-coated glass substrate remains without fog after being kept above boiling water for several minutes, contrary to the uncoated glass substrates. The superhydrophilic silica coating spreads the water droplets, which are condensed on the surface, leading to smooth drainage off the surface. This behavior can significantly aid in the increased transmission and self-cleaning effect when applied in solar PV application rainwater, and fog accumulation leads to a reduction in the power output.

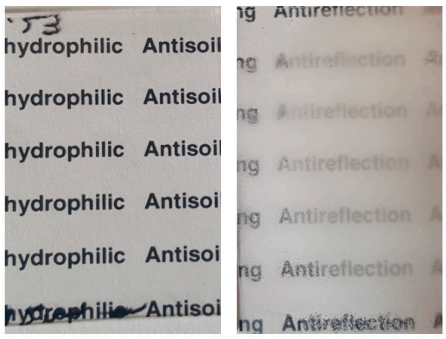

(**a**) (**b**)

Figure 5. Antifogging results: (**a**) coated glass slide; (**b**) uncoated glass slide.

3.5. Water Contact Angle

Water contact angle is a parameter used to determine the extent of wettability of a surface. Surperhydrophobic surfaces with a large water contact angle (WCA) usually greater than 150° and low rolling angle hysteresis may be used to allow water droplets to roll off the surface, cleaning the dust or soil contaminants [24,25]. Similarly, a superhydrophilic surface with a contact angle below 10° spreads the falling water droplet on its surface, cleaning the dust or soil particles from it. As shown in the Figure 6, the WCA value for the substrate decreased from 55° to 2° when a silica nanoparticle coating was introduced on the glass substrate. This shows that the surface becomes superhydrophilic, which can be used as a self-cleaning surface for a variety of applications. The presence of a hydroxyl group (OH) can be a possible explanation for the development of superhydrophilic properties in the silica nanoparticle coatings, as discussed in the FTIR analysis of the research work above [24]. Moreover, surface roughness has also been found to induce superhydrophilic behavior, as per Wenzel's theory given in Equation (6):

$$\cos \theta_w = r \cos \theta_y \quad (6)$$

where r is a measure of the roughness of the surface, called roughness factor, while θ_y and θ_w represent Young and Wenzel contact angles, respectively, encompassing the impact of topography of the surface and its chemistry to wettability; θ_w usually decreases with increasing roughness for hydrophilic materials. Simply put, surface roughness enhances the hydrophilic behavior [25,26]. In silica nanoparticles, thin film water droplets seep into the roughness spacing via 3D capillary effect. This mechanism leads to decrease in the apparent WCA.

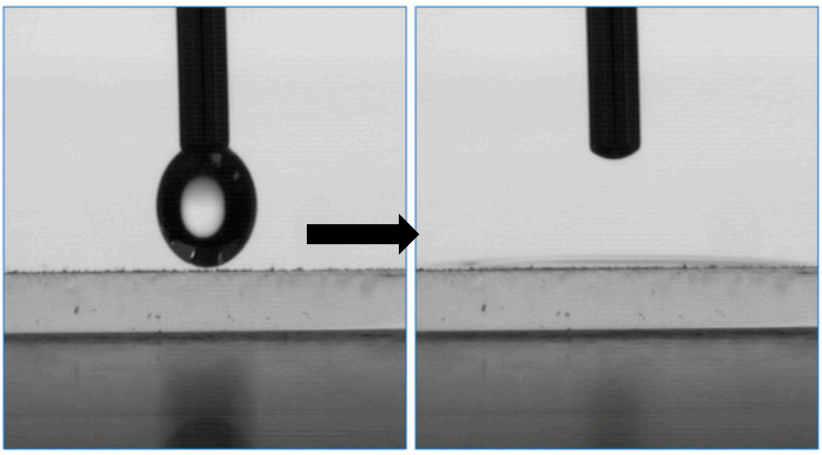

Figure 6. Water contact angle of the coated film.

3.6. Surface Morphology

Bruker nano-atomic force microscopy was used to study the surface topography of the coatings, with dimensions of 10 nm tip size and swept area of 2 μm by 2 μm, while frequency was kept at 512 Hz. AFM scanning was carried out in five different positions, giving a root mean squared (rms) roughness of 28.5 nm. Before AFM, an ellipsometer was used to determine the porosity, thickness, and refractive index of the thin film. Ellipsometry is a technique used in optical characterization of thin films. The Cauchy model was used to extract film thickness and refractive index, while a Bruggeman effective-medium approximation was used to determine porosity of the film. Measured values of pie (ϕ) and delta (Δ) were plotted against the wavelength in the range of 300–1800 nm and then fitting was done with the model. Measurement was taken at five different angles (55°, 60°, 65°, 70°, and 75°) to determine the results with ideal approximation. Figure 7a,b shows the fitting graphs used to determine the refractive index, porosity, and thickness of the thin film. The data fitted in the model and results of the optical model are shown in Figure 7c. The determined porosity, thickness and roughness of the film were 51.3% 121.24 nm, and 29.8 nm, respectively. The SEM and AFM images confirm these values

with (±5%) error of measurement. Figure 7d shows the result of measurement of refractive index with wavelength. It is clear from the graph that the refractive index is 1.23 at 600 nm. The thickness of the thin film was also confirmed by scanning electron microscope (SEM) imaging. Also interesting to note is the fact that the development of porosity inevitably leads to higher surface roughness in thin films as shown in Figure 8, invariably leading to higher wettability, as given by Wenzel's equation [20]. AFM analysis also suggests that increase in surface roughness did not adversely affect the transmittance because it was below 50 nm, as surface roughness of higher than the wavelength of the incident light scatters the light that further reduces the transmission of the substrate [5].

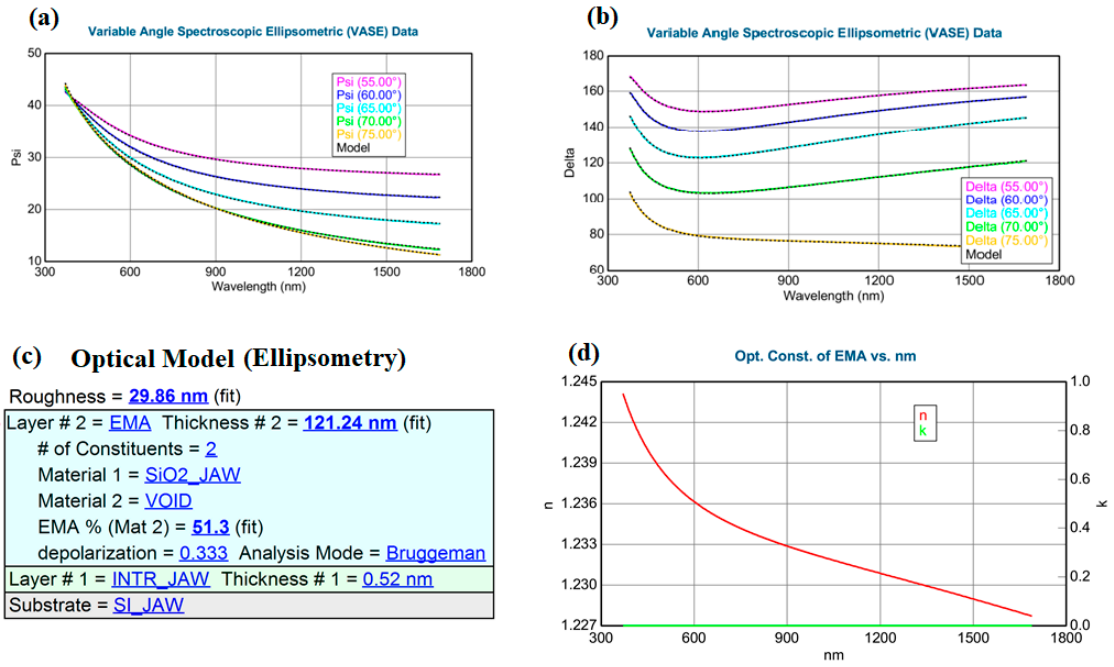

Figure 7. (**a**) Spectroscopic ellipsometry results of coated film, (**b**) showing that the experimental and generated model data fit well with each other, and (**c**,**d**) showing the optical model result, the measured porosity, roughness, and refractive index, which are 51%, 29.86 nm, and 1.23 at 600 nm, respectively.

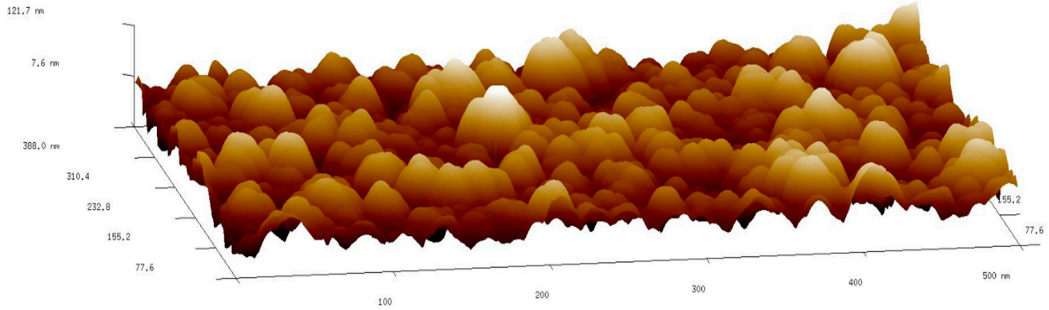

Figure 8. Surface topology by AFM.

SEM images of the surface structure of the silica nanoparticle thin film are shown in Figure 9. Figure 9a shows the surface morphology of the coating, while Figure 9b shows the cross-sectional image of the coating. It is evident from Figure 9a that the surface of the coating is nano-porous, with nanoparticles of 12.5 nm on average. It was found from the size distribution of the particles that 75% –80% of the particles were in the range of the 12–13 nm. Just 10% of the particles were above 15 nm. Also worth noting is the uniformly distributed nanopores on the surface. The increased porosity and the larger vacant spaces are the reason for the decrease in the refractive index from 1.46 to 1.23 that enhanced the optical transmittance of the glass. The cross-sectional image of SEM on the right side in

the Figure 9b shows that the thickness of the thin film coating is around 120–130 nm, as stated in the introduction portion. The surface roughness is also clear from the cross sectional image of SEM, which helps in the wettability of the surface, making it more superhydrophilic. The EDX graph (Figure 10) shows the peaks of silicon and oxygen with other small trace elements, showing that the coating is mainly comprised of silica nanoparticles, as reported by Goswami [41], Nakaso [42] Musić [43], and Wang [44] in their work. The result is consistent with previous work. The presence of very small traces of other elements in the EDX graph are due to contamination and handling problems.

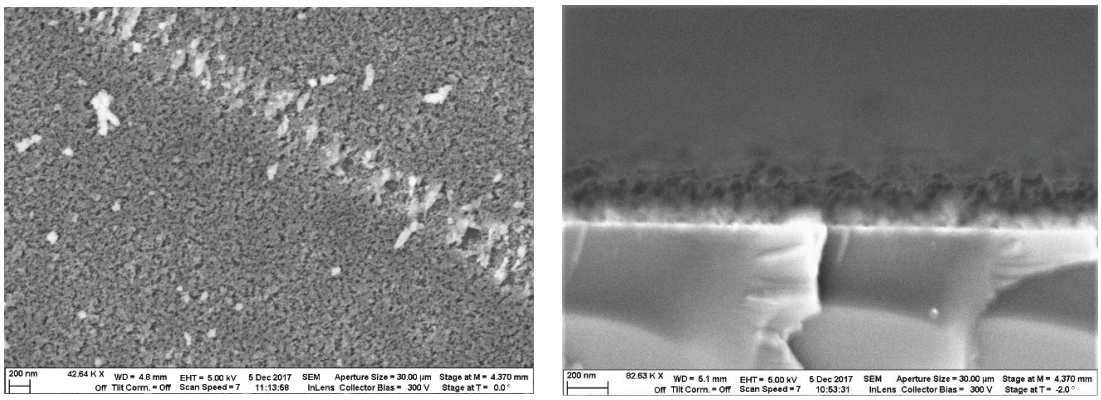

(**a**) (**b**)

Figure 9. Scanning electron micrograph (SEM) images of (**a**) surface and (**b**) cross-section.

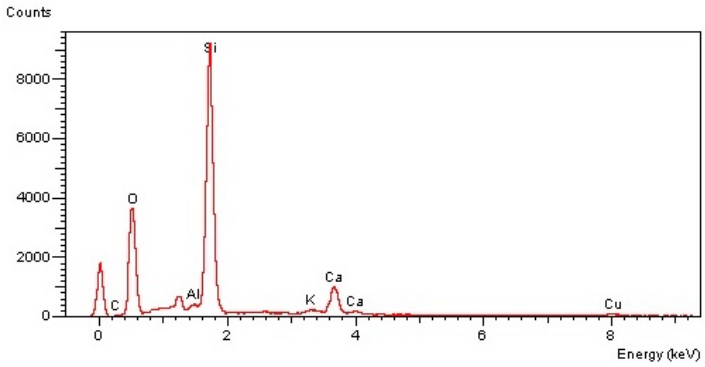

Figure 10. EDX graph of coating.

4. Conclusions

In conclusion, we have demonstrated that the aerosol spray deposition method is a simple and facile, scalable, bottom-up technology for fabrication of self-cleaning antireflection coating of SiO_2 porous nanoparticles on various substrates, including glass, polycarbonate, and silicon wafer. The thickness and porosity of the coated film can be finely tuned with the number of deposition cycles, residence time of the particles inside the reactor chamber, and flow rates of precursors, respectively. The system is not only capable of synthesizing the nanoparticles at different sizes but also has the ability to coat nanoparticles of different materials, such as titania, ZnO, and gold, depending upon precursors used in the system. The porous thin film coated glass enhances the transmittance to over 99%, which is significantly higher than the conventional cover glass of solar panels, which has a transmittance of 91%–92%. The increase in roughness and porosity of the thin film surface gave the glass substrate optically transparent and antifogging properties, enabling the solar cell to entrap 7% more light. Additionally, the coatings showed high transparency, and super-wettability to control soiling and dust accumulation on the PV module. This approach may be applicable to low cost, large-scale fabrication of AR coatings on surfaces of solar cells. For practical applications, fabrication

costs must be considered. Thus, it is believed that a solar module with coated front glass of such high transmittance will trap more light, resulting in higher electrical efficiency.

Author Contributions: Investigation, experimental work, and writing—original draft preparation, K.A., S.A.; writing—review and editing, A.S., M.H., Maoz; resources, M.S. (Muhammad Salman), M.S. (Muhammad Sadiq); project administration and funding, M.A.

Funding: This research work is funded primarily by USAID through the U.S.–Pakistan center for Advanced Studies in Energy program, under award AID-391-A-15-00001.

Acknowledgments: The authors wish to thank the researchers whose literature has been cited in this article and acknowledge Advance Materials for Energy Laboratory (Pakistan) for providing materials and experimental setups used in this study. Research leading to this article was supported by U.S.–Pakistan Center for Advanced Studies in Energy (USPCAS-E), University of Engineering and Technology (UET) Peshawar, Photovoltaic Reliability Lab (PRL ASU), Holman Research Group of ASU, and U.S. Agency for International Development, USAID.

Conflicts of Interest: The authors declare no conflict of interest.

References

1. Arabatzis, I.; Todorova, N.; Fasaki, I.; Tsesmeli, C.; Peppas, A.; Li, W.X.; Zhao, Z. Photocatalytic, self-cleaning, antireflective coating for photovoltaic panels: Characterization and monitoring in real conditions. *Sol. Energy* **2018**, *159*, 251–259. [CrossRef]
2. Kensuke, N.; Moe, S.P.; Ota, Y. Long-term reliability evaluation of silica-based coating with antireflection effect for photovoltaic modules. *Coatings* **2019**, *9*, 49. [CrossRef]
3. Shao, T.; Tang, F.; Sun, L.; Ye, X.; He, J.; Yang, L.; Zheng, W. Fabrication of antireflective nanostructures on a transmission grating surface using a one-step self-masking method. *Nanomaterials* **2019**, *9*, 180. [CrossRef] [PubMed]
4. Chen, T.; Kuo, T.; Lin, Y.; Ku, C.; Yang, Z.; Yu, I. Enhancement for potential-induced degradation resistance of crystalline silicon solar cells via anti-reflection coating by industrial PECVD methods. *Coatings* **2018**, *8*, 418. [CrossRef]
5. He, L.; Ouyang, M.; Chen, B.; Zhu, Q.; Wu, J.; Lou, N.; Dong, L.; Wang, Z.; Fu, Y. Design and fabrication of moth-eye subwavelength structure with a waist on silicon for broadband and wide-angle anti-reflection property. *Coatings* **2018**, *8*, 360. [CrossRef]
6. Viti, L.; Politano, A.; Vitiello, M.S. Black phosphorus nanodevices at terahertz frequencies: Photodetectors and future challenges. *APL Materials* **2017**, *5*, 035602. [CrossRef]
7. Politano, A.; Argurio, P.; Di Profio, G.; Sanna, V.; Cupolillo, A.; Chakraborty, S.; Arafat, H.A.; Curcio, E. Photothermal membrane distillation for seawater desalination. *Adv. Mater.* **2017**, *29*, 1603504. [CrossRef] [PubMed]
8. Gugliuzza, A.; Politano, A.; Drioli, E. The advent of graphene and other two-dimensional materials in membrane science and technology. *Curr. Opin. Chem. Eng.* **2017**, *16*, 78. [CrossRef]
9. Marco, M.; Minero, C. Quantification of the photocatalytic self-cleaning ability of non-transparent materials. *Materials* **2019**, *12*, 508. [CrossRef]
10. Joel, L.; Kherani, N. Design of nano-porous multilayer antireflective coatings. *Coatings* **2017**, *7*, 134. [CrossRef]
11. Miguel, G.; Marroyo, L.; Lorenzo, E.; Pérez, M. Soiling and other optical losses in solar-tracking PV plants in navarra. *Prog. Photovolt. Res. Appl.* **2011**, *19*, 211–217.
12. Kursawe, M.; Anselmann, R.; Hilarius, V.; Pfaff, G. Nano-particles by wet chemical processing in commercial applications. *J. Sol-Gel Sci. Technol.* **2005**, *13*, 71–74. [CrossRef]
13. Xi, J.Q.; Schubert, M.F.; Kim, J.K.; Schubert, E.F.; Chen, M.; Lin, S.-Y.; Liu, W.; Smart, J.A. Optical thin-film materials with low refractive index for broadband elimination of Fresnel reflection. *Nat. Photonics* **2007**, *1*, 176–179. [CrossRef]
14. Nogueira, G.M.; Banerjee, D.; Cohen, R.E.; Rubner, M.F. Spray-layer-by-layer assembly can more rapidly produce optical-quality multi stack hetero structures. *Langmuir* **2011**, *27*, 7860–7867. [CrossRef] [PubMed]
15. Thompson, C.S.; Fleming, R.A.; Zou, M. Transparent self-cleaning and antifogging silica nanoparticle films. *Sol. Energy Mater. Sol. Cells* **2013**, *115*, 108–113. [CrossRef]
16. Zhou, G.; He, J. Antireflective coatings on Fresnel lenses by spin-coating of solid silica nanoparticles. *J. Nanosci. Nanotechnol.* **2013**, *13*, 5534–5541. [CrossRef] [PubMed]

17. Shimomura, H.; Gemici, Z.; Cohen, R.E.; Rubner, M.F. Layer-by-layer-assembled high performance broadband antireflection coatings. *ACS Appl. Mater. Interfaces* **2010**, *2*, 813–820. [CrossRef]
18. Kim, J.-H.; Fujita, S.; Shiratori, S. Design of a thin film for optical applications, consisting of high and low refractive index multilayers, fabricated by a layer-by layer self-assembly method. *Colloids Surf. A* **2006**, *284*, 290–294. [CrossRef]
19. Prevo, B.G.; Hon, E.W.; Velev, O.D. Assembly and characterization of colloid-based antireflective coatings on multi-crystalline silicon solar cells. *J. Mater. Chem.* **2007**, *17*, 791–799. [CrossRef]
20. Vicente, G.S.; Bayon, R.; German, N.; Morales, A. Surface modification of porous antireflective coatings for solar glass covers. *Sol. Energy* **2011**, *85*, 676–680. [CrossRef]
21. Xin, D.; Xing, Y.; Zhou, M.; Li, X.; Huang, H.; Meng, X.; Wen, Y.; Zhang, X. Broadband antireflective superhydrophilic antifogging nano-coatings based on three-layer system. *Microporous Mesoporous Mater.* **2018**, *255*, 84–93.
22. Latthe, S.S.; Gurav, A.B.; Maruti, C.S.; Vhatkar, R.S. Recent progress in preparation of superhydrophobic surfaces: A review. *J. Surf. Eng. Mater. Adv. Technol.* **2012**, *2*, 76–94.
23. Zhang, Y.L.; Xia, H.; Kim, E.; Sun, H.B. Recent developments in superhydrophobic surfaces with unique structural and functional properties. *Soft Matter* **2012**, *8*, 11217–11231. [CrossRef]
24. Celia, E.; Darmanin, T.; de Givenchy, E.T.; Amigoni, S.; Guittard, F. Recent advances in designing superhydrophobic surfaces. *J. Colloid Interface Sci.* **2013**, *402*, 1–18. [CrossRef]
25. Valipour, M.N.; Birjandi, F.C.; Sargolzaei, J. Super-non-wettable surfaces: A review. *Colloids Surf. A* **2014**, *448*, 93–106. [CrossRef]
26. Aytug, T.; Lupini, A.R.; Jellison, G.E.; Joshi, P.C.; Ivanov, I.H.; Liu, T.; Wang, P.; Menon, R.; Trejo, R.M.; Lara-Curzio, E.; et al. Monolithic graded-refractive-index glass-based antireflective coatings: Broadband/omnidirectional light harvesting and self-cleaning characteristics. *J. Mater. Chem. C* **2015**, *3*, 5440–5449. [CrossRef]
27. Zhang, X.P.; Lan, P.J.; Lu, Y.H.; Li, J.; Xu, H.; Zhang, J.; Lee, Y.; Rhee, J.Y.; Choy, K.L.; Song, W.J. Multifunctional antireflection coatings based on novel hollow silica-silica nanocomposites. *ACS Appl. Mater. Interfaces* **2014**, *6*, 1415–1423. [CrossRef] [PubMed]
28. Wang, N.; Xiong, D.S. Comparison of micro-/nano-hierarchical and nano-scale roughness of silica membranes in terms of wetting behavior and transparency. *Colloids Surf. A* **2014**, *446*, 8–14. [CrossRef]
29. Wang, N.; Xiong, D.S. Superhydrophobic membranes on metal substrate and their corrosion protection in different corrosive media. *Appl. Surf. Sci.* **2014**, *305*, 603–608. [CrossRef]
30. Xu, L.; Geng, Z.; He, J.; Zhou, G. Mechanically robust, thermally stable, broadband antireflective, and super hydrophobic thin film on glass substrates. *ACS Appl. Mater. Interfaces* **2014**, *6*, 9029–9035. [CrossRef]
31. Söz, C.K.; Yilgör, E.; Yilgör, I. Influence of the average surface roughness on the formation of super hydrophobic polymer surfaces through spin-coating with hydrophobic fumed silica. *Polymer* **2015**, *62*, 118–128.
32. Hsieh, C.-T.; Wu, F.-L.; Yang, S.-Y. Superhydrophobicity from composite nano/microstructures: Carbon fabrics coated with silica nanoparticles. *Surf. Coat. Technol.* **2008**, *202*, 6103–6108. [CrossRef]
33. Cai, S.; Zhang, Y.L.; Zhang, H.L.; Yan, H.W.; Lv, H.B.; Jiang, B. Sol-gel preparation of hydrophobic silica antireflective coatings with low refractive index by base/acid two-step catalysis. *ACS Appl. Mater. Interfaces* **2014**, *6*, 11470–11475. [CrossRef] [PubMed]
34. Min, W.L.; Jiang, B.; Jiang, P. Bioinspired self-cleaning antireflection coatings. *Adv. Mater.* **2008**, *20*, 3914–3918. [CrossRef]
35. Powell, M.J.; Quesada-Cabrera, R.; Taylor, A.; Teixeira, D.; Papakonstantinou, I.; Palgrave, R.G.; Sankar, G.; Parkin, P.I. Intelligent multifunctional VO_2/SiO_2/TiO_2 coatings for self-cleaning, energy-saving window panels. *Chem. Mater.* **2016**, *28*, 1369–1376. [CrossRef]
36. Park, J.-J.; Kim, D.; Lee, J.; Kim, D.; Oh, J.; Seong, T.; van Hest, M.F.A.M.; Yoon, S. Superhydrophilic transparent titania films by supersonic aerosol deposition. *J. Am. Ceram. Soc.* **2013**, *96*, 1596–1601. [CrossRef]
37. Mangolini, L.; Thimsen, E.; Kortshagen, U. High-yield plasma synthesis of luminescent silicon nanocrystals. *Nano Lett.* **2005**, *5*, 655–659. [CrossRef] [PubMed]
38. Khardani, M.; Bouaïcha, M.; Bessaïs, B. Bruggeman effective medium approach for modelling optical properties of porous silicon: Comparison with experiment. *Phys. Status Solidi C* **2007**, *4*, 1986–1990. [CrossRef]

39. Johs, B.; Woollam, J.A.; Herzinger, C.M.; Hilfiker, J.N.; Synowicki, R.A.; Bungay, C.L. Overview of variable-angle spectroscopic ellipsometry (VASE): II. Advanced applications. In *Optical Metrology: A Critical Review, Proceedings of SPIE's International Symposium on Optical Science, Engineering, and Instrumentation, Denver, CO, USA, 18–23 July 2019*; Al-Jumaily, G.A., Ed.; SPIE: Bellingham, WA, USA, 1999.
40. Rahman, I.A.; Vejayakumaran, P.; Sipaut, C.S.; Ismail, J.; Chee, C.K. Size-dependent physicochemical and optical properties of silica nanoparticles. *Mater. Chem. Phys.* **2009**, *114*, 328–332. [CrossRef]
41. Goswami, D.; Medda, S.K.; De, G. Superhydrophobic films on glass surface derived from trimethylsilanized silica gel nanoparticles. *ACS Appl. Mater. Interfaces* **2011**, *3*, 3440–3447. [CrossRef]
42. Nakaso, K.; Han, B.; Ahn, K.H.; Choi, M.; Okuyama, K. Synthesis of non-agglomerated nanoparticles by an electrospray assisted chemical vapor deposition (ES-CVD) method. *J. Aerosol Sci.* **2003**, *34*, 869–881. [CrossRef]
43. Musić, S.; Filipović-Vinceković, N.; Sekovanić, L. Precipitation of amorphous SiO_2 particles and their properties. *Braz. J. Chem. Eng.* **2011**, *28*, 89–94. [CrossRef]
44. Wang, S.; Liu, C.; Liu, G.; Zhang, M.; Li, J.; Wang, C. Fabrication of superhydrophobic wood surface by a sol–gel process. *Appl. Surf. Sci.* **2011**, *258*, 806–810. [CrossRef]